Influence of stochasticity on multiple four-wave-mixing processes in an optical fiber

Bhaskar Khubchandani,[1,2] Parvez N. Guzdar,[2] and Rajarshi Roy,[1,2,3]
[1]*Department of Physics, University of Maryland, College Park, Maryland 20742*
[2]*IREAP, University of Maryland, College Park, Maryland 20742*
[3]*IPST, University of Maryland, College Park, Maryland 20742*
(Received 27 August 2002; published 18 December 2002)

In this paper, we present the results of a computational study of the dynamical evolution of multiple four-wave-mixing processes in a single mode optical fiber with spatially and temporally δ-correlated phase noise. A generalized nonlinear Schrödinger equation (NLSE) with stochastic phase fluctuations along the length of the fiber is solved using the split-step Fourier method. A good agreement is obtained with previous experimental and computational results based on a truncated-ODE (ordinary differential equation) model, in which stochasticity was seen to play a key role in determining the nature of the dynamics. The full NLSE allows for simulations with high frequency resolution (60 MHz) and frequency span (16 THz) compared to the truncated-ODE model (300 GHz and 2.8 THz, respectively), thus enabling a more detailed comparison with observations. A physical basis for this hitherto phenomenological phase noise is discussed and quantified.

DOI: 10.1103/PhysRevE.66.066609 PACS number(s): 42.81.−i, 05.45.Ac, 05.45.Tp, 05.45.Xt

I. INTRODUCTION

The understanding of nonlinear processes in optical fibers is crucial towards extending the capabilities of modern optical communication systems based on wavelength division multiplexing, where each communication channel is represented by a unique wavelength. One of the nonlinear processes that limits the information carrying capacity of a WDM system is four-wave mixing (FWM), which causes cross talk between neighboring channels. This places a lower limit on the wavelength separation between adjacent channels and an upper limit on the input power in each channel. In this paper, we describe a process, by which the evolution of FWM processes in an optical fiber can be used to estimate the inhomogeneities in the fiber core material, in particular, the fluctuations in the linear refractive of the fiber core.

Experiments measuring the evolution of FWM processes along a length of fiber were carried out by Hart *et al.* [1] and are described in detail in Sec. II. In this experiment, two input pump waves at frequencies ω_1 and ω_2 interacted with each other through the third-order nonlinearity of the fiber material to generate first-order sidebands at frequencies $\omega_3 = 2\omega_1 - \omega_2$ and $\omega_4 = 2\omega_2 - \omega_1$. These waves further interacted to produce second-order sidebands at $\omega_5 = 2\omega_3 - \omega_4$ and $\omega_6 = 2\omega_4 - \omega_3$. Higher-order sidebands were also generated. The normalized power in the sideband at frequency ω_m was represented by ρ_m. The evolution of the FWM processes was characterized by the evolution of $\rho_m(z)$ as a function of fiber length z.

In the present work, we make a quantitative comparison between these experimental results and our numerical results based on efficient algorithms [2] to solve the nonlinear Schrödinger equation (NLSE) that governs the system. The numerical model, its underlying assumptions and the results are described in Sec. III. A realistic description of a standard single mode optical fiber must take into account the random phase perturbations a light wave undergoes while propagating through it, without disturbing the underlying conservative properties of the system. The NLSE needs to be suitably modified in order to incorporate the stochastic nature of the propagation. In order to preserve the conservative properties of the system, the stochastic terms in the NLSE must necessarily be multiplicative in nature as an additive term acts as a source or a sink. An algorithm that achieves this with linear, Gaussian, δ-correlated noise is outlined in Sec. III. This algorithm preserves the unconditional stability of the system. At the same time, care is taken to transform the stochastic NLSE from its original Ito representation [3] to the computationally feasible Stratanovich representation [4] by compensating for the spurious linear drift that results from integrating such stochastic differential equations [5–8]. The dominant sources of phase noise are discussed in Sec. IV.

Conclusions on the relevance of the experiments of Hart *et al.* [1] and the stochastic modeling presented here are summarized in Sec. V.

II. EXPERIMENTAL AND COMPUTATIONAL BACKGROUND

In this work, we focus on tracing the evolution of the sidebands, generated through FWM, along a length of optical fiber. The FWM spectral evolution along 50 m of fiber for two input pump power regimes (2.1 W and 5.5 W) was investigated. In the 2.1 W case, the sideband evolution followed a damped sinusoid along the length of the fiber. The experiments also found that the two first-order sidebands (ρ_3 blueshifted and ρ_4 redshifted from the two pumps) had different evolutions along the fiber (with different spatial wavelengths). For the 5.5 W case, the evolution of both first- and second-order sidebands was measured. The damping in the first-order sidebands (ρ_3 and ρ_4) occured faster than in the 2.1 W case. Experiments probing the dependence of the sideband power on the input power (ranging from 2 W to 17 W) were also performed at a fixed output length of 50 m of the fiber. At the same fiber length, the optical spectra for input powers ranging from 2 W to 17 W were also recorded. The spectral envelopes were observed to fit well to a hyperbolic secant function and the fit parameters were recorded. Mea-

surements with a high-resolution wavemeter showed that one of the two pumps consisted of two very closely spaced longitudinal modes ($\Delta\nu \sim 0.5$ GHz), which were not resolved by the spectrometer used to record the FWM spectra. Inclusion of this multimode nature of the pump input in their model was found to alter the sideband dynamics dramatically and partly explained the asymmetry between the blue-shifted and redshifted sidebands though it did not account for the damping in the sidebands. This was accounted for by adding weak phase fluctuations to the waves as they propagated along the fiber. The physical source of these phase fluctuations was not known at that time. However, the inclusion of the phase fluctuations into the model gave excellent qualitative and quantitative agreement with experiment. Their model involved integration of a system of coupled ODEs (ordinary differential equations) derived from the NLSE [9] by a process of truncation that retained only the leading frequency components (the pumps and the first- and second-order sidebands), a process justified by the fact that the input pump waves are well approximated by a combination of monochromatic waves. Their final numerical results are based on simulations using the truncated-ODE model with Langevin noise terms representing phase fluctuations in the fiber. Another physical source of stochasticity in their experiment was the inherent power fluctuation in the lasers used as the input pumps. The level of fluctuations (5–20%) was measured and incorporated appropriately into their model through stochastic initial conditions. This explained the evolution of the level of observed fluctuations in the sideband trajectories although it was found to be inadequate by itself to account for the damping of the trajectories. They found that all the three physical characteristics mentioned above, namely, the multimode nature of the pump input, the stochastic phase fluctuations along the length of the fiber, and the stochastic initial power fluctuations were crucial towards explaining the different features of the experimental measurements.

III. STOCHASTIC-NLSE MODEL

In the present work, we have developed and implemented an unconditionally stable scheme for integrating the NLSE that successfully incorporates phase noise into the split-step Fourier method (SSFM). Thus, we are now in a position to harness, the high frequency/time resolution of the SSFM, together with its efficient convergence properties. Due to these advances, we are now able to do simulations with much higher frequency resolution (60 MHz as compared to 300 GHz in the ODE model). This high resolution, coupled with an appropriate convolution scheme enables us to compare these simulated spectra with the composite spectra observed by the spectrometers which had a resolution of $\sim$60 GHz. This was not possible with the truncated- ODE model as the resolution of the simulated spectra in that case was $\sim$300 GHz. For exactly the same levels of phase fluctuations and initial condition fluctuations as used in Ref. [1], comparisons for the present NLSE model with the experimental sideband evolution functions $\rho_i(z)$ show excellent quantitative agreement. These results, along with the algorithms employed are described in detail in this section. We have identified linear refractive index fluctuations along the fiber length to be a strong candidate for a physical source of the stochastic phase fluctuations. A comparison between the various possible sources is given in Sec. IV.

Under the assumption that the electric field of the light in the fiber has a slowly varying envelope $A(z,\tau)$, and that the fiber medium has an instantaneous nonlinear response, the system is well described by the NLSE with a linear multiplicative stochastic term,

$$\frac{\partial U}{\partial z} + \frac{i\beta^{(2)}}{2T_0^2}\frac{\partial^2 U}{\partial \tau^2} + \frac{\alpha U}{2} + i\Gamma(z,\tau)U - i\gamma P_0|U|^2 U = 0. \tag{1}$$

Z is the distance along the length of the fiber, $U(z,\tau) = A(z,\tau)/\sqrt{P_0}$ is the complex electric field envelope $A(z,\tau)$ normalized to the absolute amplitude of the field $\sqrt{P_0}$, P_0 is the total power in the fiber, τ is time normalized to a convenient time scale $T_0(\sim 1$ ns) measured in a reference frame moving with the group velocity of the pulse $[\tau=(t - z/v_g)/T_0]$. The simulations are carried out for exactly the same physical parameters as the experiments and simulations reported by Hart *et al.* [1], i.e., $\beta^{(2)} = 55$ ps^2/km is the group velocity dispersion of the fiber at the operating wavelength $\lambda_0 \sim 632$ nm ($k_0 \sim 10^7$ m^{-1}). $\alpha \sim 6$ dB/km$=0.0014$ m^{-1} is the loss in the fiber at this wavelength. The nonlinearity coefficient $\gamma = 0.019$ W^{-1} m^{-1} is given by

$$\gamma = \frac{\omega_{av} n_2^I}{c A_{eff}}, \tag{2}$$

where A_{eff} is the effective core area of the fiber, n_2^I is the Kerr coefficient for the intensity-dependent refractive index, and ω_{av} is the average angular frequency of the wave envelope. $\Gamma(z,\tau)$ is a linear multiplicative phase noise field. In this study the noise field is assumed to be δ correlated in both space and time. The evolution of the FWM dynamics is found to be sensitive to the strength of this noise field. It can be physically interpreted as phase noise arising due to fluctuations in the linear refractive index of the fiber medium. A detailed discussion of its physical origin is given in Sec. IV.

The system was simulated using the SSFM [2]. An algorithm for appropriately incorporating stochastic phase fluctuations along the length of the fiber in the SSFM was developed and is summarized below.

The NLSE is composed of linear and nonlinear terms, and can be written in the operator form as

$$\frac{\partial U}{\partial z} = (\hat{D} + \hat{S} + \hat{N})U,$$

$$\hat{D} = \frac{-i\beta^{(2)}}{2T_0^2}\frac{\partial^2}{\partial \tau^2} - \frac{\alpha}{2},$$

$$\hat{S} = i\Gamma(z,\tau),$$

$$\hat{N} = i\gamma P_0|U|^2, \tag{3}$$

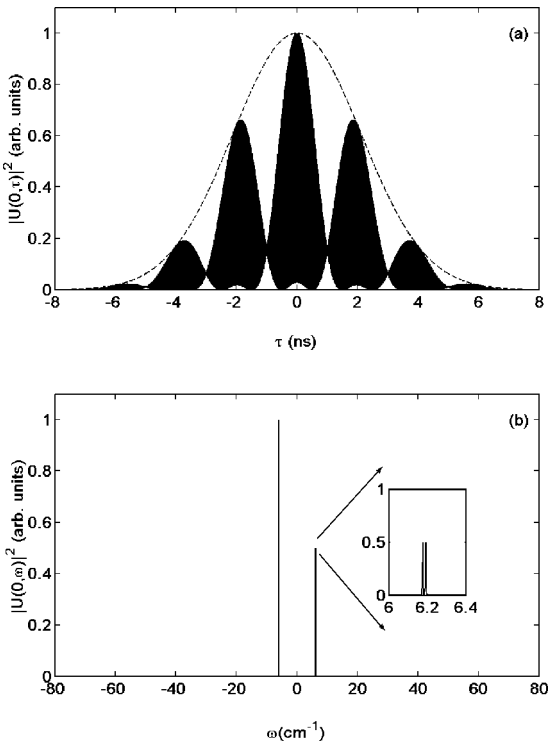

FIG. 1. Multimode pulse input to the NLSE: (a) input pulse in time domain and (b) input spectrum.

where $\hat{D}$, $\hat{S}$, and $\hat{N}$ are linear (dispersive), nonlinear, and stochastic operators, respectively. It has an exact solution for infinitesimal Δz given by

$$U(z+\Delta z,\tau)=\exp[\Delta z(\hat{D}+\hat{S}+\hat{N})]U(z,\tau), \tag{4}$$

which can be approximated by

$$U(z+\Delta z,\tau)\approx\exp[\Delta z\hat{D}]\exp[\Delta z\hat{S}]\exp[\Delta z\hat{N}]U(z,\tau). \tag{5}$$

The execution of $\exp[\Delta z\hat{N}]$ is carried out in τ space:

$$B_1(z,\tau)=\exp[\Delta z\hat{N}]U(z,\tau). \tag{6}$$

The execution of $\exp[\Delta z\hat{S}]$ and $\exp[\Delta z\hat{D}]$ is carried out in ω space.

In particular, the stochastic phase fluctuations are introduced by modifying the phase ϕ_j of each frequency component ω_j of the complex field according to

$$B_2(z,\omega)=\mathcal{F}[B_1(z,\tau)],$$

$$B_3(z,\omega_j)=\exp[i\delta\phi(z,\omega_j)]B_2(z,\omega_j), \tag{7}$$

where $\mathcal{F}$ represents the Fourier transform operation.

This process only modifies the phase of each complex frequency component leaving its absolute value unchanged. Thus, the algorithm conserves the total power and the unconditional stability of the system.

The stochastic phase fluctuations $\delta\phi(z,\omega_j)$ are taken to be δ correlated in frequency as well as along the fiber length. The Box-Muller algorithm [10] was used to generate Gaussian random deviates from computer-generated uniform random deviates r_{1j} and r_{2j} at each spatial step and for each frequency component ω_j. The fluctuations are given by

$$\delta\phi(z,\omega_j)=\sqrt{-2\sigma_\phi^2\Delta z\ln(r_{1j})}\cos(2\pi r_{2j}). \tag{8}$$

This is followed by the execution of $\exp[\Delta z\hat{D}]$ which is also carried out in Fourier space followed by the inverse transform:

$$U(z+\Delta z,\tau)=\mathcal{F}^{-1}[\exp[\Delta z\hat{D}(i\omega)]B_3(z,\omega)]. \tag{9}$$

$\hat{D}(i\omega)$ is obtained by replacing $(\partial/\partial\tau)$ by $i\omega$.

The basic form of the initial complex wave envelope function is

$$U(0,\tau)=\exp\left(-\frac{\tau^2}{2\tau_p^2}\right)\left\{\exp\left(\frac{i\Omega\tau}{2}\right)+\exp\left(-\frac{i\Omega\tau}{2}\right)\right\}. \tag{10}$$

τ_p is the pulse width $T_p=5$ ns FWHM (full width at half maximum), normalized to the time scale T_0, $\Omega=366$ GHz is the frequency detuning between the two laser sources normalized to a frequency scale $\Omega_0=62.5$ MHz. Figure 1(a) shows a plot of this pulse $|U(0,\tau)|^2$. The overall Gaussian envelope has an FWHM of 5 ns, the closely spaced dark lines are due to the 366 GHz ($\sim$3 ps) beating between the two input pump frequencies. The 2-ns modulations on the pulse are due to the 0.5-GHz mode structure in the blue-shifted pump wave. Figure 1(b) shows the input spectrum of this pulse, which consists of two highly monochromatic pump waves with a detuning of $\Omega=366$ GHz. The spectrum of the blue-shifted pump, upon magnification, is seen to be composed of two very closely spaced peaks, with a separation of $\Delta\nu=0.5$ GHz. Hart *et al.* [1] did not use pulsed wave functions in their NLSE simulations as the size of the FFT required to do so made it computationally prohibitive at that time. The size of the (FFT) was chosen such that it would accommodate a time span of 16 ns in order to go sufficiently far into the wings on the Gaussian pulse; and a frequency span of 16 THz in order to accommodate all the sidebands generated and prevent spurious effects due to the reflection boundary conditions implicit in the SSFM algorithm. These considerations dictated the size of the FFT to be $\geqslant$16 THz $\times$16 ns$=$256 000. The nearest power of 2 is $2^{18}=262\,144$, which has been used throughout the present work. The incorporation of the pulsed nature of the light was found to be necessary in explaining the dynamics. From the perspective of the coupled amplitude equations used by Hart *et al.* [1], the present model is equivalent to a coupled-ODE model with 2^{18} coupled ODEs.

Upon incorporation of the multimode nature of the blue input pump-laser source and the stochastic fluctuations in the initial power in the lasers, the initial wave function takes the form

$$U(0,\tau)=\exp\left(-\frac{\tau^2}{2\tau_p^2}\right)\left\{\sqrt{\frac{1+\delta\rho_1}{2}}\left[\exp\left(\frac{i(\Omega+\Delta\nu)\tau}{2}\right)+\exp\left(\frac{i(\Omega-\Delta\nu)\tau}{2}\right)\right]+\sqrt{1+\delta\rho_2}\exp\left(-\frac{i\Omega\tau}{2}\right)\right\}. \tag{11}$$

$\Delta\nu=0.5$ GHz is the frequency separation between the two longitudinal modes in the blue-shifted pump. $\delta\rho_1$ and $\delta\rho_2$ are Gaussian random deviates (generated using the Box-Muller algorithm [10]) that represent the initial power fluctuations in each of the pump laser sources. Their standard deviations were taken to be $\sigma_{\rho_1}=0.2$, $\sigma_{\rho_2}=0.11$ for simulations from 0 m to 20 m, $\sigma_{\rho_1}=0.12$, $\sigma_{\rho_2}=0.05$ for simulations from 20 m to 50 m along the length of the fiber. This is exactly the same prescription used by Hart *et al.* [1] in their simulations and is dictated by their experimental measurements of the fluctuations in the pump-laser intensities.

Use of the FFT algorithm makes evaluation relatively fast compared to other finite-difference schemes. The computational error is $O(\Delta z^2)$, thus the solution converges with decreasing spatial step size Δz.

The simulations were tested for the conservation of total power along the fiber length (by setting the loss α to zero) and for the conservation of asymmetry [1,9] given by

$$C(Z)=\sum_{i=1}^{\infty}(2i-1)[\rho_{2i-1}(Z)-\rho_{2i}(Z)]. \tag{12}$$

A clear picture of the evolution of the sidebands is obtained by plotting the power in the sidebands as a function of length along the fiber. Figures 2(a) and 2(b) show a comparison between simulation and experiment of the evolution of the first-order blue (ρ_3) and red (ρ_4) sidebands, respectively, for an input power of 2.1 W. The solid line in the figure is generated by numerical solution of the stochastic NLSE. The measured sideband power, normalized to the total power in the fiber, is periodic in length, but appears to be damping to a constant value. The measured data also show a clear difference between the spatial wavelengths of oscillation of the blue and red sidebands trajectories, respectively. Both these features are captured well by the simulations. Figures 2(c) and 2(d) compare experimental and simulated measures of the evolution of the standard deviation in the sideband power along the fiber length.

The apparent damping of the periodic sideband trajectory is seen more dramatically in Figs. 3(a) and 3(b), which show the evolution of the first-order sideband power along the fiber for an input power of 5.5 W. Here again, the two first-order sidebands evolve differently. They also appear to damp to a constant value at a faster rate than for the case with an input pump power of 2.1 W. All of these features are accurately captured by the stochastic-NLSE model. Figures 3(c) and 3(d) show a comparison between the simulated and measured standard deviations. Comparisons for the second-order blue (ρ_5) and red (ρ_6) sidebands, respectively, are shown in Figs. 3(e) and 3(f).

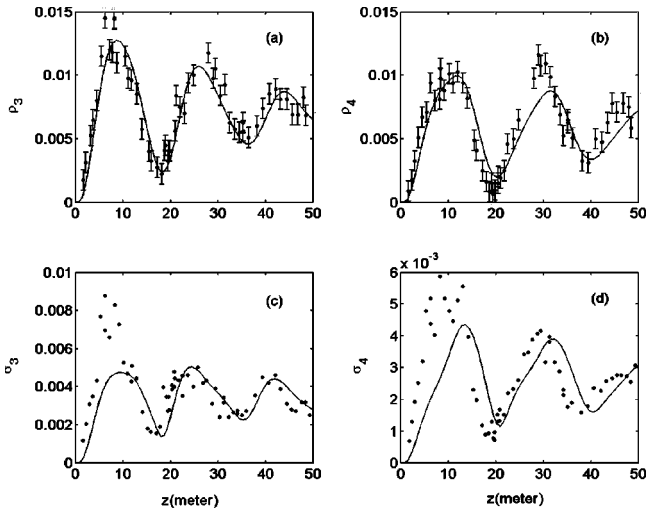

FIG. 2. Comparison between the experimental measurements [1] and the stochastic-NLSE model (solid line) of the first-order sideband evolution as a function of fiber length for $P_0=2.1$ W, $\Omega=366$ GHz, $\Delta\nu=0.5$ GHz, $\gamma=0.019$ W^{-1} m^{-1}, and $\beta^{(2)}=55$ ps^2/km: dynamical evolution of the (a) power in the blue-shifted sideband, (b) power in the redshifted sideband, (c) fluctuations in the blue-shifted sideband, (d) fluctuations in the redshifted sideband.

The observed dynamical evolution of the sidebands is found to depend sensitively on the strength of the stochastic phase fluctuations. Yet, best agreement with the experimental results of Hart *et al.* [1] is achieved with exactly the same noise strength σ_ϕ^2 as used in their truncated-ODE model,

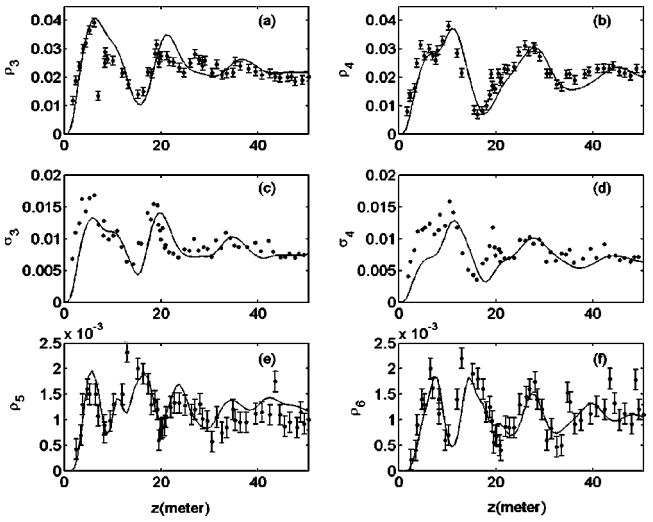

FIG. 3. Comparison between the experimental measurements [1] and the stochastic-NLSE model (solid line) of the first- and second-order sideband evolution as a function of fiber length for $P_0=5.5$ W, $\Omega=366$ GHz, $\Delta\nu=0.5$ GHz, $\gamma=0.019$ W^{-1} m^{-1}, and $\beta^{(2)}=55$ ps^2/km: dynamical evolution of the: (a) power in the first-order blue-shifted sideband, (b) power in the first-order redshifted sideband, (c) fluctuations in the first-order blue-shifted sideband, (d) fluctuations in the first-order redshifted sideband, (e) power in the second-order blue-shifted sideband, (f) power in the second-order redshifted sideband.

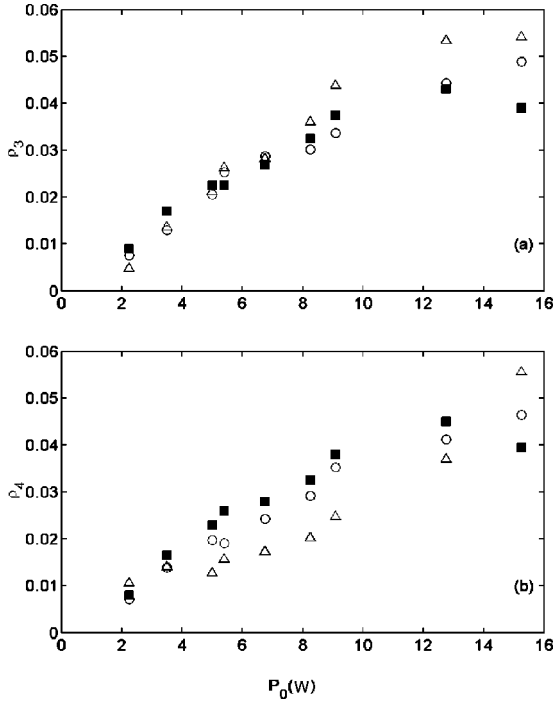

FIG. 4. Comparison between the experimental measurements (stars) and the stochastic-NLSE model (open symbols) of the first-order sideband power versus pump input power for $L=50.39$ m and $\Omega=366$ GHz: power in the (a) blue-shifted sideband and (b) red-shifted sideband.

namely, $\sigma_\phi^2=0.0067$ m^{-1}. They report that including phase noise in their FWM calculations resulted in a spurious linear drift in the trajectories for the sideband power with length. To remove this artifact of the computations, they added a linear loss to their coupled ODEs. They set the loss coefficient $\alpha=0.0046$ m^{-1} by finding the value that removed this increasing slope. We have observed exactly the same secular growth phenomenon for a wide range of the noise strength σ_ϕ^2 and have arrived at an empirical prescription for α, namely, $\alpha\sim\sigma_\phi^2$, where σ_ϕ^2 is the variance of the added phase noise. This indicates the general nature of dynamics resulting from the addition of stochastic, δ correlated phase fluctuations to systems governed by nonlinear partial differential equations [5].

It is remarkable that the strength of the phase noise required is the same in both the 2.1 W and the 5.5 W cases. Further, it is worth noting that exactly the same noise strength was used by Hart *et al.* [1], the difference being that they introduced phase noise only in the pump frequencies, whereas we have introduced it in all the Fourier modes ($\sim 2^{18}$). As a confirmation of this result, they also performed experiments and numerical simulations examining the sideband power dependence on the input power at a fixed length of 50.4 m of the same fiber. We have repeated these simulations with the stochastic-NLSE model and the results are shown in Figs. 4(a) (blue-shifted sideband) and 4(b) (red-shifted sideband). The experimental measurements of the sideband powers are represented by filled squares and the results of numerical simulations are represented by triangles

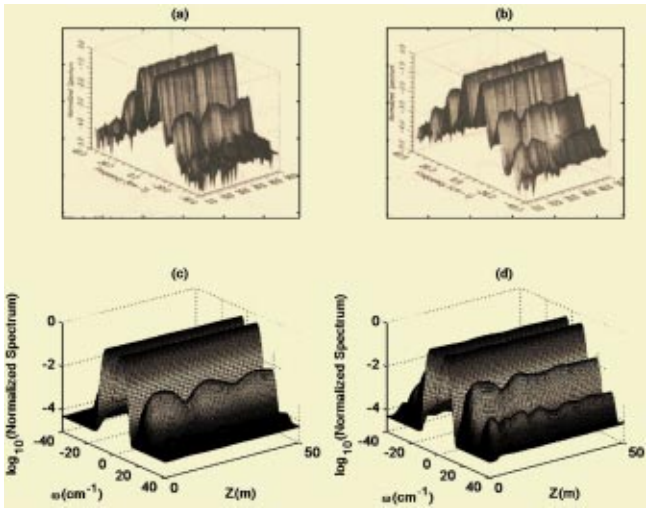

FIG. 5. Evolution of the FWM spectrum along the fiber (a) $P=2.1$ W, experiment; (b) $P=5.5$ W, experiment, (c) $P=2.1$ W, stochastic-NLSE model; (d) $P=5.5$ W, stochastic-NLSE model.

(without phase noise) and by circles (with phase noise). The simulations are seen to follow the general trend seen in the experiments. As the pump power is increased, the triangles (without phase noise) start to disagree with experiment, whereas the circles (with phase noise) are much closer to experiment. The phase noise strength used in these simulations was exactly the same as that used in the simulations depicted in Figs. 2 and 3. The agreement between the phase noise simulations and the experimental data was (once again) highly sensitive to the noise strength. Since this experiment (unlike those shown in Figs. 2 and 3) is nondestructive, it can be used to deduce the strength of phase noise processes in a given optical fiber. It will be shown in Sec. IV that a likely cause of the phase noise is fluctuation in the linear refractive index of the fiber. The noise strength deduced from the present computational study corresponds to a refractive index inhomogeneity of $\langle\Delta n^2\rangle\sim 10^{-16}$.

Till now, the comparisons between our simulations of the full-NLSE and the truncated-ODE model give basically the same results, although in a much better agreement with experiment. However, the full NLSE can also provide a detailed comparison with the experimental spectra. This was not available from the truncated-ODE model. The simulations reported in this work were carried out with a very high frequency and time resolution in order to incorporate the fact that the input light was not cw, but was composed of $\sim$5-ns long pulses; and that the number of sidebands generated required the frequency spread of the FFT to be $\sim$16 THz, while resolving a longitudinal mode structure of $\Delta\nu$ $\sim$0.5 GHz. The spectral resolution used was $\sim$0.05 GHz, whereas the spectrometer used to observe the spectra had a resolution 1000 times larger ($\sim$50 GHz) To account for this difference, the simulated spectra were first convolved with a Gaussian of unit peak and 62-GHz FWHM, before they were compared with the observed spectra.

Figures 5(a) and 5(b) show three-dimensional plots of the average experimental FWM output spectrum along the length of the fiber for input pump powers of 2.1 W and 5.5

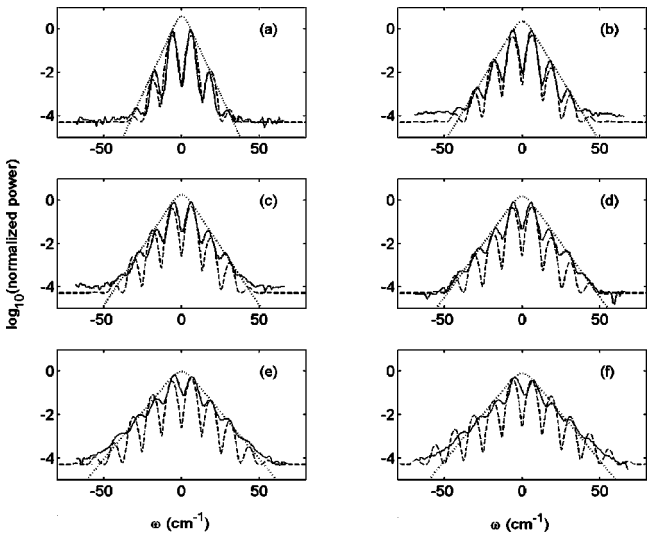

FIG. 6. Experimental FWM output spectrum (solid line), convolved spectra from simulations of the stochastic-NLSE model (dashed line), and hyperbolic secant envelope fit (dotted line) for pump input powers P_0 of (a) 2.1 W, (b) 5.5 W, (c) 6.7 W, (d) 8.3 W, (e) 12.7 W, (f) 17.4 W, fiber length $L=50.39$ m, $\Omega=366$ GHz, $\Delta\nu=0.5$ GHz, $\gamma=0.019$ W^{-1} m^{-1}, and $\beta^{(2)}=55$ ps^2/km.

W respectively (courtesy Hart *et al.* [1]). The vertical axis represents the intensity, normalized to the peak power in one of the input pumps, plotted on a logarithmic scale. The pump frequencies are centered on $+/-\Omega/2$ and the fiber length is increasing into the page. Figures 5(c) and 5(d) show the corresponding comparisons based on simulations using the stochastic-NLSE model. The basic features of the spectral evolution are captured by the simulations.

Hart *et al.* [1] also documented the experimentally observed FWM output spectra for a fixed fiber length of 50.39 m for six different input pump powers. They state the coefficients A and B of the hyperbolic secant envelopes that best fit the output spectra which are given by

$$f(\omega)=A\,\mathrm{sech}(B\omega), \tag{13}$$

where A and B are the experimental fit parameters.

The hyperbolic secant parameters A and B that best fit the simulated spectra are exactly the same as those that best fit the experimental spectra [1] for all the six cases of input power considered. Figure 6 shows an overlap of the simulated spectra (dashed line), with the experimental spectra (solid line) and the experimental hyperbolic secant envelope (dotted line) for six different pump powers, namely, (a) 2.1 W, (b) 5.5 W, (c) 6.7 W, (d) 8.3 W, (e) 12.7 W, (f) 17.4 W. The hyperbolic secant parameters for each of these pump powers are (a) $A=3.85$ and $B=0.36$, (b) $A=2.26$ and $B=0.27$, (c) $A=1.81$, and $B=0.25$, (d) $A=1.56$ and $B=0.23$, (e) $A=0.98$, and $B=0.20$ and (f) $A=0.81$ and $B=0.20$. The exact shapes of the simulated spectra match very well with the experimental spectra for low input pump powers (2.1 W and 5.5 W) but tend to lack the ''filled-in'' character of the experimental spectra at higher powers (6.7 W, 8.3 W, 12.7 W, and 17.4 W).

IV. DISCUSSION

Hart *et al.* [1] postulated that strong candidates for the possible physical sources of the phase fluctuations are stimulated Brillouin scattering, stimulated Raman scattering and fiber medium inhomogeneities. Brillouin scattering was eliminated as a source, since a backward propagating wave, which is a signature of Brillouin scattering in optical fibers, was not observed in the experiments. We have modeled stimulated Raman scattering [2,11] for our system and have found no evidence to support the hypothesis that it could be a possible source of the stochastic phase fluctuations. Apart from these, quantum phase fluctuations are another well known, though extremely weak, source of phase noise in optical fibers [2,13].

Fiber medium inhomogeneities were identified as the major cause of the stochastic phase fluctuations. These inhomogeneities can manifest themselves through spatial and/or temporal fluctuations in the fiber parameters, namely, the linear refractive index n_0, the group velocity v_g, the group velocity dispersion $\beta^{(2)}$, and the nonlinearity γ [12]. Of these, the fluctuation in the linear refractive index was found to be the only source of phase fluctuation that had a significant effect on the dynamics. A relationship between the level of refractive index fluctuations and the corresponding level of phase fluctuations has been arrived at. It is found that refractive index fluctuations as small as $\sigma_n^2\sim10^{-17}$ m^{-1} can cause the desired phase fluctuations. Possible sources of these refractive index fluctuations are discussed below.

Consider the modified nonlinear Schrödinger equation (NLSE) which is stated below, with the linear multiplicative noise term represented in terms of spatial and temporal fluctuations in the refractive index of the fiber:

$$\frac{\partial U}{\partial z}+\frac{i\beta^{(2)}}{2T_0^2}\frac{\partial^2 U}{\partial\tau^2}+\frac{\alpha U}{2}+ik_0\delta n(z,\tau)U-i\gamma P_0|U|^2U=0. \tag{14}$$

$\delta n(z,\tau)$ is the spatial and temporal variation of the refractive index along the fiber. It can be caused by temperature and density fluctuations in the fiber [14].

The thermodynamic estimate for Δn is given [14] by

$$\langle\Delta n^2\rangle=\frac{-kT\rho^2}{V^2}\left(\frac{\partial V}{\partial P}\right)_T\left(\frac{\partial n}{\partial\rho}\right)_T^2+\frac{kT^2}{\rho VC_v}\left(\frac{\partial n}{\partial T}\right)_\rho^2. \tag{15}$$

This gives the mean-square index fluctuation in terms of the properties of the material. It can be rewritten as

$$\langle\Delta n^2\rangle=\frac{V_\rho+V_T}{V}=\langle\Delta n^2\rangle_\rho+\langle\Delta n^2\rangle_T. \tag{16}$$

For a fiber of length $z=1$ m and radius $r=2.82$ μm (volume $V=2.5\times10^{-12}$ m^3), these have been calculated to be

$$\langle\Delta n^2\rangle_\rho\sim10^{-21}\equiv\langle\Delta\rho^2\rangle\sim10^{-14}\frac{\mathrm{kg}^2}{\mathrm{m}^6},$$

$$\langle\Delta n^2\rangle_T\sim10^{-23}\equiv\langle\Delta T^2\rangle\sim10^{-12}\,^\circ\mathrm{C}^2. \tag{17}$$

It should be noted that $\langle \Delta n^2 \rangle \propto 1/z \Rightarrow \delta n \propto 1/\sqrt{z}$. The corresponding phase fluctuation that this would lead to in the NLSE is given by $\delta\phi = k_0 \delta n z \propto \sqrt{z}$, which is equivalent to the prescription for incorporating phase fluctuations into the stochastic NLSE model described in Sec. III, namely, $\langle \Delta \phi^2 \rangle = 6.7 \times 10^{-3} z$. Hart *et al.* [1] used the same prescription and the same noise strength in their truncated-ODE model. From this, we can estimate the level of refractive index fluctuation that corresponds to the noise strength used in the simulations described in Sec. III:

$$\langle \Delta n^2 \rangle = \frac{6.7 \times 10^{-3}}{k_0^2} = 6.78 \times 10^{-17} \equiv \langle \Delta T^2 \rangle \sim 10^{-6} {}^\circ\mathrm{C}^2$$

$$\equiv \Delta T \sim 10^{-3} {}^\circ\mathrm{C}. \tag{18}$$

The temperature coefficient of the refractive index of silica [14], $(\partial n/\partial T)_\rho \sim 10^{-5}\,{}^\circ\mathrm{C}^{-1}$. Thus even small spatiotemporal temperature fluctuations of $\sim 10^{-3}\,{}^\circ\mathrm{C}$ are enough to cause the inferred level of refractive index fluctuations.

The refractive index fluctuations could also be due to inhomogeneities in the density of the fiber material, frozen in at the time of manufacture of the fiber. The simulations were averaged over ~ 600 iterations to get a good estimate of the power fluctuations in the sidebands. Initially, simulations were performed with a different phase noise distribution for each iteration. Later, a particular (arbitrary) phase noise distribution was selected and frozen for all the iterations. This did not reduce the level of damping observed in the sideband trajectories provided that the strength of the phase noise was kept the same, thus indicating that density fluctuations induced during fiber manufacture could be a possible source. The phase noise was modeled as δ correlated in both space and time. A more realistic approach would be to use correlated noise. Numerical methods to incorporate linear multiplicative correlated noise into the NLSE have been developed by Werner *et al.* [6].

V. CONCLUSIONS

The role of stochasticity in the dynamical evolution of four-wave-mixing processes in an optical fiber has been investigated. This research consisted of theoretical and numerical computations. It focuses on tracing the evolution of the sidebands, generated through FWM, along a length of optical fiber. Detailed comparisons were made with the experimental results of Hart *et al.* [1] and the agreement was excellent. The present work uses numerical techniques that have much higher resolution and better efficiency, and it presents a theoretical basis for the role of the stochasticity in the dynamics. The system is known to be governed by the (NLSE) to a very good approximation [2].

A powerful technique that can be used for simulations of the stochastic NLSE is the split-step Fourier Method (SSFM) [2]. An algorithm for the direct implementation of stochastic processes along the length of the fiber in the SSFM has been developed. The advantages of this approach with respect to the coupled-ODE approach are that we can carry out simulations with much higher frequency and time resolution without sacrificing computational efficiency.

The physical sources of these stochastic phase fluctuations are investigated quantitatively and are identified to be due to fluctuations in the linear refractive index of the fiber. Strong candidates for the causes of these refractive index fluctuations are temperature fluctuations in the fiber medium caused by the fluctuating temperature of the fiber environment, density fluctuations in the fiber medium frozen into the fiber during manufacture, and intrinsic thermodynamic fluctuations in the temperature and density of the fiber.

The experiments performed by Hart *et al.* [1] can be used to determine the level of these refractive index fluctuations in commercial fibers. Results described in Figs. 2 and 3 represent a destructive experiment that measures the sideband evolution with fiber length for fixed input pump power, necessarily requiring the fiber to be cut repeatedly. The level of refractive index fluctuations can be used as a parameter in the simulations to best fit the experimental results. Alternatively, Fig. 4 represents a nondestructive experiment that measures the sideband evolution with input pump power for a fixed fiber length. These experiments are found to be effective for estimating the refractive index fluctuations as the dynamics is observed to be sensitively dependent on the strength of the phase fluctuations.

ACKNOWLEDGMENT

We gratefully acknowledge support from the Office of Naval Research (Physics).

[1] D.L. Hart, Arthur F. Judy, Rajarshi Roy, and James W. Beletic, Phys. Rev. E **57**, 4757 (1998); D.L. Hart, Arthur F. Judy, T.A.B. Kennedy, Rajarshi Roy, and K. Stoev, Phys. Rev. A **50**, 1807 (1994).

[2] G.P. Agrawal, *Nonlinear Fiber Optics* (Academic, San Diego, 2001).

[3] K. Ito, *Lectures on Stochastic Processes* (Tata Institute of Fundamental Research, Bombay, 1960).

[4] R.L. Stratanovich, *Topics in the Theory of Random Noise* (Gordon & Breach, New York, 1963), Vols. I and II.

[5] H. Risken, *The Fokker-Planck Equation* (Springer-Verlag, Berlin, 1989).

[6] M.J. Werner and P.D. Drummond, J. Comput. Phys. **132**, 312 (1997).

[7] P.D. Drummond and I.K. Mortimer, J. Comput. Phys. **93**, 144 (1991).

[8] S.J. Carter, Phys. Rev. A **51**, 3274 (1995).

[9] J.R. Thompson and Rajarshi Roy, Phys. Rev. A **43**, 4987 (1991).

[10] W.H. Press, S.A. Teukolsky, W.T. Vetterling, and B.P. Flannery, *Numerical Recipes in Fortran: The Art of Scientific Computing* (Cambridge University Press, Cambridge, 1992).

[11] C. Headley and G.P. Agrawal, IEEE J. Quantum Electron. **QE-31**, 2058 (1995); J. Opt. Soc. Am. B **13**, 2170 (1995).

[12] F.Kh. Abdullaev, J.H. Hensen, S. Bischoff, and M.P. Sorensen, J. Opt. Soc. Am. B **15**, 2424 (1998); F.Kh. Abdullaev, J.G. Caputo, and Nikos Flytzanis, Phys. Rev. E **50**, 1552 (1994).
[13] S.H. Perlmutter, M.D. Levenson, R.M. Shelby, and M.B. Weissman, Phys. Rev. Lett. **61**, 1388 (1988).
[14] William H. Glenn, IEEE J. Quantum Electron. **QE-25**, 1218 (1989).